Supplementary Information

Self-assembled Cellulose Nanofiber-Carbon Nanotube Nanocomposite Films with Anisotropic conductivity

Anne Skogberg*, Sanna Siljander*, Antti-Juhana Mäki, Mari Honkanen, Alexander Efimov, Markus Hannula, Panu Lahtinen, Sampo Tuukkanen, Tomas Björkqvist and Pasi Kallio

1.1 Electrical measurements and stability of the nanocomposite

For each nanocomposite film type (S1, S2, S3 and control), there were three parallel films and the resistance measurement (Figure 3) was repeated three times for each individual film in order to show the repeatability of the presented assembly. The average resistance of the parallel films and the repeat measurements (n=9) are summarized in Figure S1 with a 95% confidence interval.
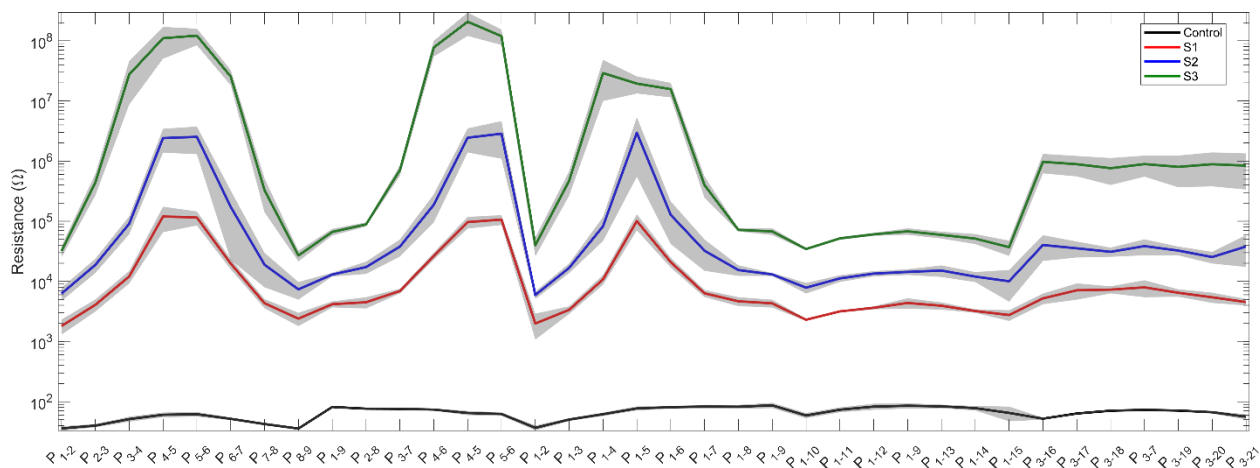
Figure S1. Resistance of parallel films and repeat measurements (n=9) of S1, S2, S3, and Control, with 95% confidence interval (shaded gray).

Measurements in Figure S1 show that we can repeatably produce assembled films (S1, S2, S3) possessing anisotropic electrical properties, as well as control films with isotropic electrical properties. In the case of assembled films, there is increased resistance towards the center of the films, while the resistance remains relatively unchanged along the studied imaginary Circles 1 and 3. Thus, the assembled films are homogeneous along the circles (along the orientation direction of

1

c-CNF), but heterogeneous along the radial line; that is, from the edge towards the center of the film. This direction is perpendicular to the orientation direction.

Concerning nanocomposite sample film stability, the same films have been measured and imaged repeated times during a long time period. Figure S2 shows the same sample film during heating tests and IR camera images on different days in time span of about half year, during which the sample shows consistent heating without changes in its properties. In addition, we report the parallel and repeat resistance measurements (Figure S1). We have repeated all the measurements at least three times. As a result, each nanocomposite were applied in electric field for at least 11 min during the resistance measurements. This was repeated three times for each film, to demonstrate stability of the films. In addition, three parallel films were fabricated in order to show the repeatability of film manufacturing. We have also used different voltages in the measurements and have observed similar heating with equal voltages once the heating was repeated. This shows that application of an electric field does not change the properties of the film. As a summary, we conclude that the anisotropic nanocomposite structure is very stable both during time, and when electric field is applied.
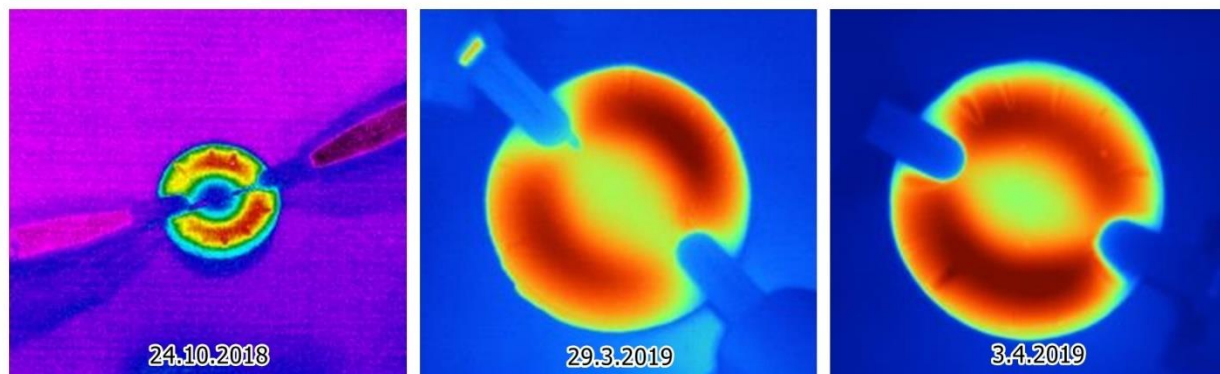
Figure S2. IR camera images of the same sample recorded on different days on a time period of half a year.

1.2 Comparison between the control sample and the assembled sample

In the manuscript, three different assembled samples S1-S3 and an isotropic control sample C was compared using thermal camera imaging, and resistance measurements (Figure 2 and Figure 3 of the manuscript, respectively). The results show the difference between anisotropic assembled and isotropic control films. However, this section provides additional data to confirm the difference

between the control and the assembled films using different samples and experiments. These consist of different dispersion concentrations and different types of electrical measurements, including IR imaging experiments, and resistance measurements.

To study the influence of the current on the temperature distribution on the film, different currents between 0.01-0.1 A were supplied to the film and the temperature distribution was detected using an IR camera. As illustrated in Figure S3, the film is evenly heated with both currents.
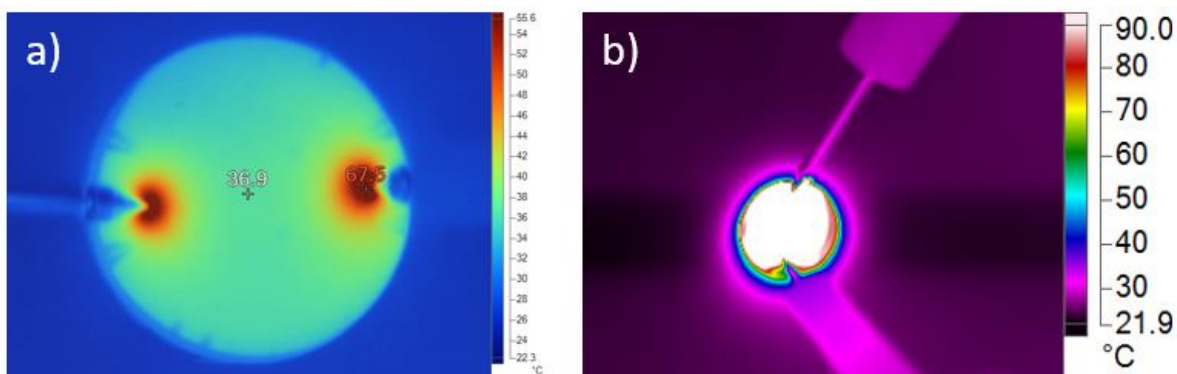
Figure S3. IR images of control samples with lower current 0.01 A (a) and higher current 0.1 A (b).

To demonstrate the difference in the electric conductivity between the control sample (without additional c-CNF) and the assembled, electrically anisotropic, films (with additional c-CNF), resistance was measured along circumferential ("Circle, R1") and radial ("Centerline, R2") directions. With electrically isotropic films, the ratio of the resistances (R2/R1) should be close to 1, while substantially different in electrically anisotropic films. In the cellulose- MWCNTs dispersions, two different concentrations of MWCNTs were used: w% of 0.05 in Sample C1 or w% 0.1 in Sample C2. The ratio (R2/R1) was determined and compared between the control samples C1 and C2 and between a control sample (C1 or C2) and assembled samples. The results show a significant difference between control and assemble samples as illustrated in Table 1.

Sample type	M2/M1
C1 + c-CNF (1)	159,1
C1 + c-CNF (2)	145,1
C1 + c-CNF (3)	214,5
C1 (1)	1,8
C1 (2)	1,8
C1 (3)	1,6
Sample type	**M2/M1**
C2 + c-CNF (1)	66,2
C2 + c-CNF (2)	76,8
C2 + c-CNF (3)	75,2
C2 (1)	1,3
C2 (2)	1,1
C2 (3)	1,3

Finally, to show the difference in the electric conductivity between the control sample (without additional c-CNF) and the assembled, electrically anisotropic, films (with additional c-CNF), resistance was measured using another dispersion batch of c-CNF and MWCNT. An example of comparison of individual measurement points between a control sample (C) and an assembled sample (S1) is presented in Table 2. The measurement points are the same as presented in the manuscript Figure 8.

Table 2. Resistance measured in different measurement locations, along the center line (Measurement A, B and C) and along the circle (Measurement D and E) and from the nanocomposite films manufactured using dispersion (sample C) and suspension (sample S1). Suspension is composed of dispersion and added c-CNF.

	Resistance (Ω)	
Measurement A	Sample C	S1
P_{1-2}	26	13 000
P_{2-3}	33	36 000
P_{3-4}	38	770 000
P_{4-5}	43	2 062 000
P_{5-6}	42	2 703 000
P_{6-7}	39	4 191 000
P_{7-8}	33	134 000
P_{8-9}	29	13 000
Measurement B		
P_{1-9}	68	32 000
P_{2-8}	61	43 000
P_{3-7}	58	160 000
P_{4-6}	53	2 158 000
P_{4-5}	44	1 903 000
P_{5-6}	43	2 314 000

	Resistance (Ω)	
Measurement C	Sample C	S1
P_{1-2}	28	13 000
P_{1-3}	41	30 000
P_{1-4}	59	595 000
P_{1-5}	62	1 382 000
P_{1-6}	62	1 187 000
P_{1-7}	62	139 000
P_{1-8}	64	40 000
P_{1-9}	66	32 000

	Resistance (Ω)	
Measurement D	Sample C	S1
$1\text{-}45°_{11}$	45	14 000
$1\text{-}45°_{12}$	41	15 000
$1\text{-}90°_{11}$	58	24 000
$1\text{-}90°_{12}$	57	25 000
$1\text{-}135°_{11}$	65	29 000
$1\text{-}135°_{12}$	68	31 000
$1\text{-}180°_{1}$	68	32 000
$3\text{-}45°_{11}$	39	78 000
Measurement E		
$3\text{-}45°_{12}$	39	100 000
$3\text{-}90°_{11}$	52	88 000
$3\text{-}90°_{12}$	53	212 000
$3\text{-}135°_{11}$	59	221 000
$3\text{-}135°_{12}$	57	232 000
$3\text{-}180°_{1}$	59	152 000

Each of the experiments indicate the same significant difference between the control and assembled samples, regardless the slight differences in the experiment setup or the samples itself.

1.3 Structural characterization of the nanocomposite films

Based on IR-imaging, we would expect higher MWCNT concentration on the film edges. However, this is not evident from the surface images (Figure S4a and e) in which MWCNTs are evenly distributed throughout the film, while the cross-section scans show variation in the MWCNT amount between the edge and the centre area (Figure S4b, f and Figure S4c, g, respectively), as well as between the control and the assembled films (Figure S4j, k and Figure S4b, c, f, g, respectively). There is a visible difference in the MWCNT portion such that it is higher in the peripheral locations (Figure S4c and g) compared to the locations close to the centre (Figure S4b and f). In addition, the concentration of MWCNTs is higher in the control film than in the assembled films.

The thickness of the film in the edge and centre locations cannot be compared using SEM imaging due to sample preparation techniques and sample angles. Therefore, the film thickness was analyzed by non-destructive micro-CT (Supplementary information 1.4). As the coffee ring effect predicts accumulation of MWCNTs on the edge of the film, it would explain increasing conductivity in the zones, that is, circles towards the periphery of the film. Thus, the hypothesis based on the coffee ring effect would expect thicker films towards the edge/periphery in the self-assembled (S1) films in contrast to a more even thickness in the control films. However, according to the micro-CT analysis, there is no such trend in the thickness of the nanocomposite films. In contrast, opposite to the coffee ring hypothesis, the control film is somewhat thicker closer to the edge than to the inner parts of the film. The self-assembled S1 film is oppositely thinner closer to the edge of the film.
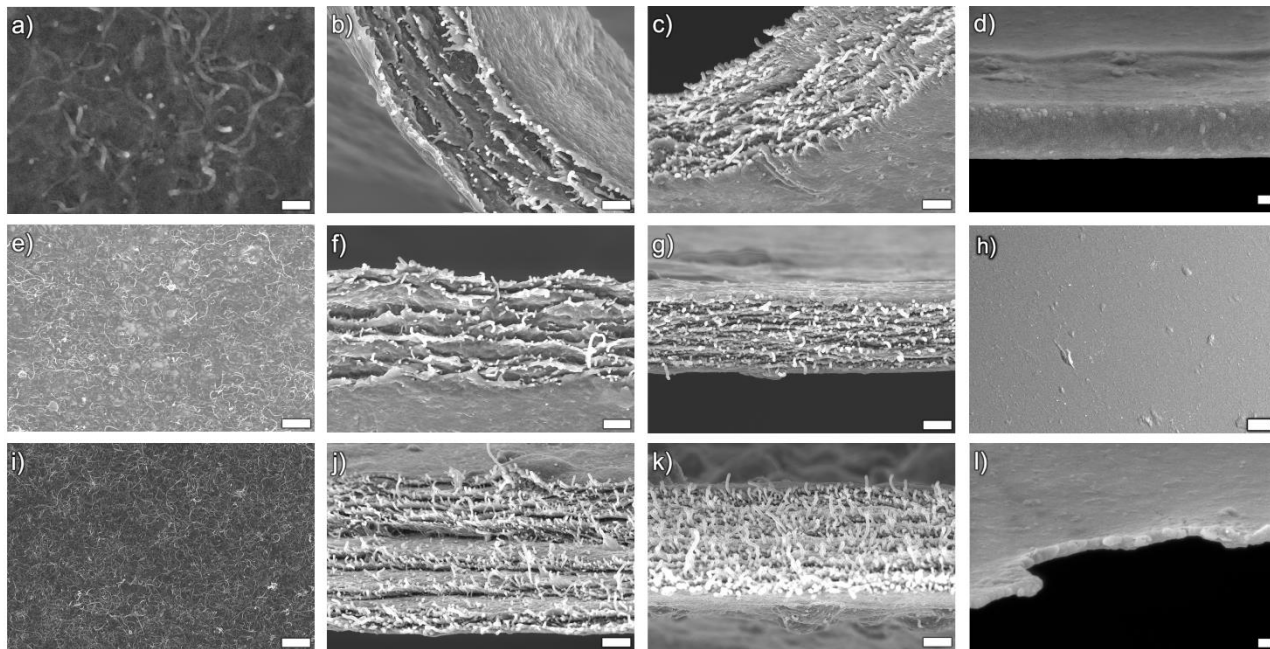
Figure S4. SEM images of the assembled films (a–h) and the control films (i–l). Surface scans with visible MWCNTs (a, e, i). Larger view surface scan of an assembled film with aligned c-CNF (h). Cross-section views of the torn film surface close to the centre location (b, f, j) and from the peripheral location, that is, closer to the edge (c, g, k). Edge view of the intact assembled (d) and control (l) nanocomposite film. Scale bar sizes are as follows: 200 nm (a, d, l), 1 µm (b, c, e, f, g, i, j, k) and 100 µm (h).

When analyzing the low vacuum SEM surface scans (one example in Figure S5), it is evident that the c-CNF fibrillates during sonication, as the larger fiber bundles that can be seen in S1 and S2 (Figure S5a-b) are missing in S3 (Figure S5c). This is due to the higher sonication energy used to fibrillate the added hes-c-CNF in S3. The sonication energy used in S3 is the same as that used to disperse hes-c-CNF/MWCNT.
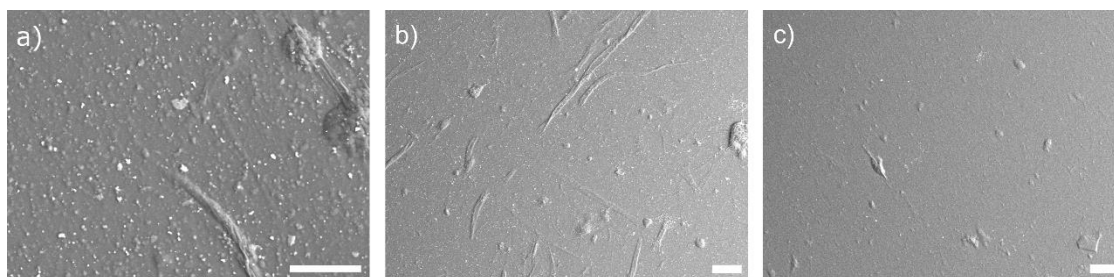
Figure S5. Low vacuum SEM from the surface of the S1 (a), S2 (b) and S3 (c) samples. The suspended c-CNF is the c-CNF supernatant in S1 and S2, while the supernatant was further sonicated 625 kJ/g (hes-c-CNF/MWCNT) before suspending it with the dispersion in S3. Scale bar sizes are as follows: 50 µm (a), and 100 µm (b, c).

1.4 Film thickness characterization using micro CT

Selected areas from the outer and inner region of the S1 and Control films were imaged with micro-computed tomography (μ-CT) and a 3D -thickness analysis was performed for the corresponding areas. The regions were determined such that the outer region covers the area of the conducting (heating) loop (Figure 2b), and the inner region is close to center. Images (Figure S6 a–b) show smooth control films compared to the assembled S1 films (Figure S6 c-d). More thickness variation is seen in S1 films, which is due to the larger fibers present in the c-CNF solution. In addition, assembly itself may result in thickness variation along the film.
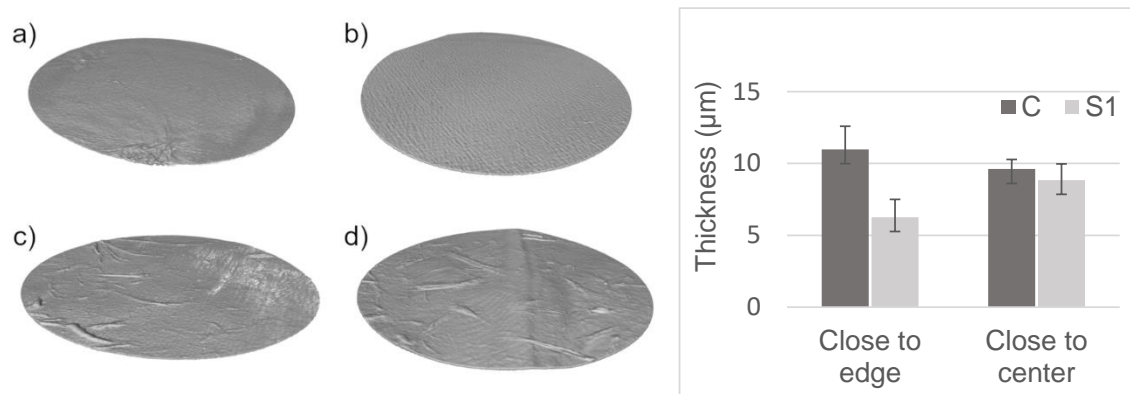
Figure S6. Micro-CT images. Control film in outer (a) and inner (b), and S1 film in outer (c) and inner (d) region. The chart presents the thickness of the control (C) and assembled (S1) films determined by microCT close to the edge and close to the center parts of the films. The studied area is 0,95 mm in diameter.

1.5 The effect of sonication treatment on chemical composition

To attain more information regarding to sonication treatments, semi-solid state MAS NMR spectroscopy, and ATR FTIR were applied. Structural characterization of the reference untreated c-CNF (Figure S7a) and the sonicated samples (Figure S7b-c for c-CNF and Figure S7d for c-CNF-MWCNT dispersion) was accomplished using NMR. The ^{1}H NMR spectra in Figure S7 show the proton signals of the untreated c-CNF (Figure S7a), which was used as a reference for the examination of the effects of sonication treatments on the sonicated samples (Figure S7b and

S7c for hes-c-CNF sonicated at energy 625 kJ/g and 1250 kJ/g, respectively, and Figure S7d for hes-c-CNF-MWCNT dispersion).

The ^{1}H NMR spectrum of untreated c-CNF (Figure S7a) and hes-c-CNF (Figure S7b-c) shows peaks at 4.4 (4.45 ppm[3]) for H8 and 3.1 (3.25[3]) for H10, which belong to the cationic substituent. The signals with an overall integral from 4.4 to 2.9 originate from the cellulose protons. The spectra were measured with water suppression (at 4.67 ppm), thus the peaks 5.5–4.5 are invisible. The degree of substitution was earlier determined to be 0.35, so the nine methyl protons H10 from the trimethylammonium group of the reacted GTAC have relatively high intensity. Further, the intensity/proportion of the signal remain relatively unchanged in all samples (Figure S7a-c), indicating that the functional group remain intact and relatively stable throughout the sonication treatments. Untreated c-CNF, hes-c-CNF sonicated with 625 kJ/g, and hes-c-CNF sonicated with 1250 kJ/g have the same signals, so the effect of sonication on the chemical structure of c-CNF is assumed negligible.

The exact interaction between c-CNF and MWCNT during sonication is not obvious from ^{1}H NMR spectra as the analyte is aggregated and signals are broad and overlapping (Figure S7d). However, when compared to the signals obtained from c-CNF alone, some conclusion can be drawn on the organization of c-CNF in the sample. The observable signals in semi-solid MAS spectra at 3.1 ppm, 3.44 ppm, and 3.55 ppm are coming from solvated fragments of the compound, that is, the corresponding functional chains should point outward, to the surrounding of the aggregated clusters. The peak at 3.1 ppm belongs to methyl protons of the trimethylammonium group. The H7 and H9 protons of the cationic substituent are non-equivalent and give two distinct signals in the spectrum NMR. However, these protons cannot be easily spotted in the spectrum of c-CNF because of overlapping with other signals.[3] Rather, it has been reported that the H7 (3.63 ppm) and H9 (3.52 ppm) protons are hidden in the region of ring-protons of the glucose residues.[4] These signals may be visible in Figure S7d, as the functional group is expected to point out from the entangled hes-c-CNF-MWCNT nanostructure. In addition, cellulose ring protons H3–H5 appear on this area,[3,5] as Jiang *et al*.[5] have determined unmodified CNF proton peaks, H3 (3.75ppm), H4 (3.66ppm), and H5 (3.52 ppm).

If H4 and H5 ring proton signals falling to the same region[3,5] would be weaker due to less solvation, the signals of H7 and H9 of the substituent would appear. However, it is not possible

from the spectra to identify which of these individual proton peaks are visible. As the peaks in the area of 5 ppm to 3.8 ppm are weak and broadened, the corresponding protons are not solvated in the measurement conditions (suspension in D_2O), which indicates a strong interaction between those areas of c-CNF with MWCNT. The formed nanostructure is tightly packed, which prevents water from penetrating between the interaction sites; this results in non-solvated regions, which are observed as weak and broad signals. In summary, as the trimethylammonium protons of cationic substituent remain unchanged in all samples, we can assume it is facing outward from MWCNT, and the less solvated area refers to cellulose ring protons, in this case some of the H3–H5, which would be the location of stronger interaction with MWCNT.
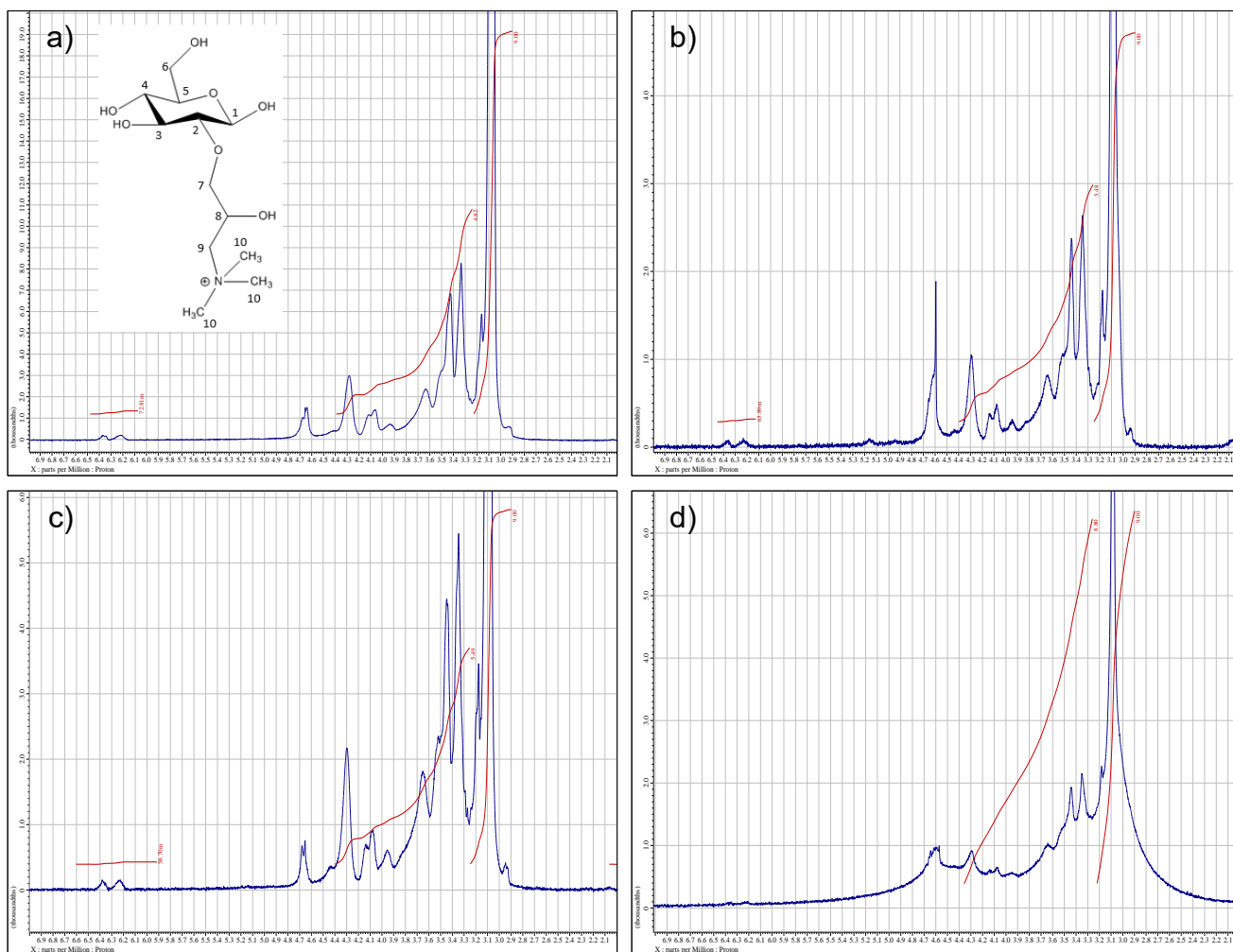
Figure S7. The FG-MAS ^{1}H NMR spectra of the untreated c-CNF (a), hes-c-CNF supernatant sonicated 625 kJ/g (b), hes-c-CNF supernatant sonicated 1250 kJ/g (c), and hes-c-CNF-MWCNT dispersion sonicated 625 kJ/g (d).

The NMR result is in accordance with the suggested interaction in which hes-c-CNF covers MWCNT (Figure 6h). It also provides valuable information about the ordering of hes-c-CNF relative to MWCNT. Thus, we can make assumptions of the dispersion chemistry that the free c-CNF encounters when suspended with the dispersion. According to NMR, there is no chemical modification of the dispersion components during sonication treatments.

It is evident from the low vacuum SEM scans (Figure S5) that the c-CNF fibrillates during sonication, as the bigger fiber bundles are missing in assembled film S3 (Figure S5c) that we see

in assembled films S1 and S2 (Figure S5a-b). This is because the sonication treatment of the added hes-c-CNF in S3, which has exactly the same sonication energy as that used disperse hes-c-CNF/MWCNT. This is due to the fibrillation occurring during stronger sonication compared to lower amount of sonication and thus less fibrillation in the case of the first step sonication of diluted c-CNF suspension, described in Methods section.

FTIR (effect of sonication on the chemical composition of c-CNF)

FTIR spectra (Bruker Tensor 27 FTIR spectrophotometer, Billerica, USA) (Figure S8) were obtained from the c-CNF samples before and after sonication for comparison of the absorption bands of the untreated and sonicated samples. The FTIR-ATR-Diamond spectra of untreated c-CNF, hes-c-CNF sonicated at 625 kJ/g, and hes-c-CNF sonicated at 1250 kJ/g exhibit absorption bands corresponding to the asymmetric –CH$_3$ stretching vibration at 1470 (1481) cm^{-1} and C-N stretching vibration at 903 (916) cm^{-1}, due to hydroxypropyltrimethylammonium groups substituted at C2 hydroxyl groups of cellulose. In addition, the adsorption bands of cellulose are observed at 1415 (1412), 1315 (1318–3320), and 903 (897) cm^{-1}, which can be assigned to the –CH$_2$ scissoring, –OH bending, O–H deformation, and β-glucopyranose ring vibrations, respectively. From the spectra, we can assume that the chemical bonds remain unchanged. This is consistent with the data obtained from NMR.
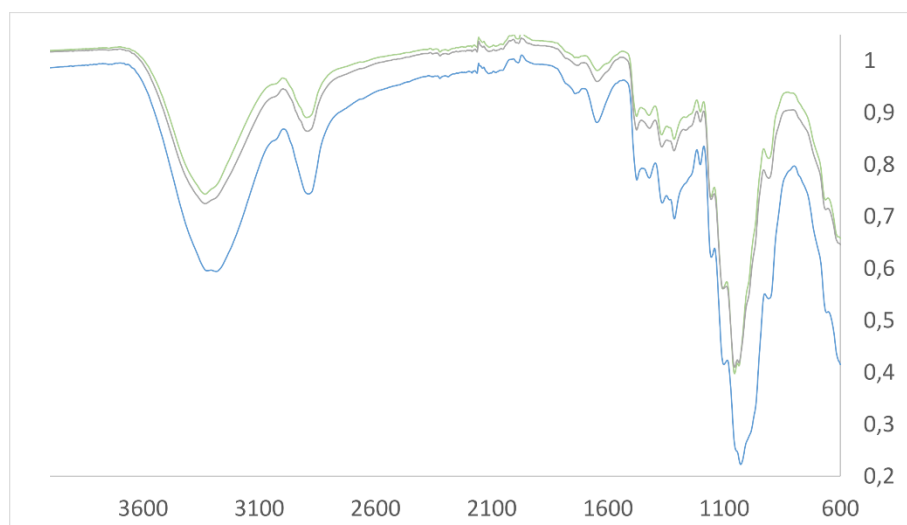
Figure S8. FTIR ATR-Diamond spectra of untreated c-CNT (blue), and c-CNF sonicated with 625 kJ/g (light green) and 1250 kJ/g (green).

References

1   K. Kartasalo, R.-P. Pölönen, M. Ojala, J. Rasku, J. Lekkala, K. Aalto-Setälä and P. Kallio, *BMC Bioinformatics*, 2015, **16**, 344.

2   A. Skogberg, A. J. Mäki, M. Mettänen, P. Lahtinen and P. Kallio, *Biomacromolecules*, 2017, **18**, 3936–3953.

3   H. De La Motte, M. Hasani, H. Brelid and G. Westman, *Carbohydr. Polym.*, 2011, **85**, 738–746.

4   A. Ebringerová, Z. Hromádková, M. Kačuráková and M. Antal, *Carbohydr. Polym.*, 1994, **24**, 301–308.

5   F. Jiang, J. L. Dallas, B. K. Ahn and Y. Lo Hsieh, *Carbohydr. Polym.*, 2014, **110**, 360–366.